Journal of Physics: Conference Series **500** (2014) 112031 doi:10.1088/1742-6596/500/11/112031

The influence of shock-loading path on the spallation response of Ta

G T Gray III[1], N K Bourne[2], V Livescu[1], C P Trujillo[1], S MacDonald[3] and P Withers[3]

[1] Los Alamos National Laboratory, Los Alamos, New Mexico, 87545, USA
[2] AWE Aldermaston, Reading, Berkshire, RG7 4PR, UK
[3] University of Manchester, Sackville Street, Manchester, M60 1QD, UK

E-mail: rusty@lanl.gov

Abstract. Spallation is well known to be a complex process strongly influenced by microstructure, loading path, and the loading profile yet often a singular "spall strength" is utilized in hydrocodes to quantify the dynamic fracture behavior of a material. In the current study, the influence of loading path on the "spall strength" and damage evolution in high-purity Ta is presented. Tantalum samples where shock loaded to three different peak shock stresses using both symmetric impact, and two different composite flyer plate configurations such that upon unloading the three samples displayed nearly identical "pull-back" signals as measured via rear-surface velocimetry. While the "pull-back" signals observed are similar in magnitude, the highest peak stressed sample resulted in complete spall scab separation while the two lower peak stresses resulted in incipient spall. The damage evolution in the "soft" recovered Ta samples was quantified using optical metallography, electron-back-scatter diffraction, and tomography. The effect of loading path on spallation and its ramifications for the stress and kinetic dependency of dynamic damage evolution is discussed.

1. Introduction

Research over the past six decades has provided a wealth of experimental data and insight concerning the influence of microstructure and shock pulse history (i.e., peak stress, pulse duration, loading and release rates, and 1-D versus complex loading) on the spallation response of materials [1-4]. Investigations by Rinehart [5], and Butcher *et al.* [6] detailed how the formation and thickness of the "scabbing under explosive loading" (*i.e.* spallation), depends on the shape of the stress wave imposed. Butcher *et al.* [6] demonstrated that "since spallation is studied by introducing a pulse and observing the effects of the tensile stresses within the material, knowledge of the complete stress history at the spall plane is necessary to the quantitative understanding of spall". Experiments by Butcher *et al.* [6] and more recently by Gray et al. [4] showed "that the spallation stress is less for square pulses than for triangular pulses" in metals displaying ductile damage evolution modes. Contrary to ductile metals where the kinetics for void initiation, growth, and linkage result in a strong dependence of spall strength on wave profile shape, the dynamic damage of tungsten heavy alloy (WHA), failing by brittle cleavage through the tungsten particles, is seen to be relatively insensitive to the shock pulse duration and accompanying unloading (tensile) pulse [7]. In this case, the brittle damage kinetics and the spall strength was dominated by the shock peak stress, independent of the shock pulse duration. The influence of non-one-dimensional oblique loading paths has also been shown to significantly affect ductile damage evolution during spallation loading in Cu [8]. High-explosive-driven sweeping-wave

loading of Ta has been observed to yield a lower spall strength than previously documented for 1-D supported-shock-wave loading and to exhibit increased shock hardening as a function of increasing obliquity [8]. The purpose of the current study was to subject Ta samples to three different peak shock stresses followed by, as close as possible, nearly identical tensile loading pulses leading to spallation damage evolution.

2. Experimental Techniques

2.1. Material

Targets for the spallation experiments were prepared from commercially pure, triple electron-beam melted and annealed tantalum plate, 10.2 mm in thickness obtained from Cabot Corporation [9]. The chemical composition (in wt%) was analyzed to be carbon 10 ppm, oxygen <50 ppm, nitrogen <10 ppm, hydrogen <5 ppm, tungsten <25 ppm, niobium <25 ppm, titanium <5 ppm, iron <5 ppm, and the balance Ta. The plate was produced from an ingot, which was forged into a billet; this was then annealed, and subsequently cut prior to cross rolling. The plates were straight rolled in the final finishing passes. The texture strength was moderate, with the <111> fiber component approximately three times random. Average grain size of this material was 35 μm. Acoustic properties of the tantalum were measured using 5 MHz quartz transducers with a Parametrics 500PR pulse receiver. The density (ρ_0) of the tantalum studied was measured to be 16.58 ± 0.01 g/cc, longitudinal sound speed (c_L) 4130 ± 30 m/s and shear sound speed (c_S) 2040 ± 30 m/s. The Poisson ratio (ν) was 0.339.

2.2. Spallation Plate Impact

The primary diagnostics for these experiments was sample recovery with post-mortem metallurgical analysis and Photon Doppler Velocimetry (PDV) [10]. Soft recovered spall plate impact experiments were conducted using a 80-mm bore gas launcher and soft-recovery techniques presented previously [11]. Three identical 4.572-mm thick right circular tantalum targets were prepared with press fit momentum trapping rings to mitigate perturbations from edge release waves. A square wave profile was achieved using a 2.25-mm thick Ta monolithic impactor impacting the spall sample at 250 m/s. The thickness of this impactor was chosen as one half that of the target to locate the spall plane at the target midline. Two higher peak stress spallation tests were conducted using composite impactors. The first composite impactor consisted of 1.27 mm of Ta backed by 4.98 mm of Al and was impacted into the target at 375 m/s while the highest stress impactor consisted of 1.18 mm of Cu backed by 1.24 mm of W and impacted into the target at 615 m/s. Impact velocities were measured to an accuracy of 1% using a sequential pressure transducer method and sample tilt was fixed to ~1 mrad by means of an adjustable specimen mount. Following impact, all samples were soft recovered by decelerating them into low-density foam. The free surface velocity (FSV) history profiles were measured using PDV single-point probes, one aimed at the sample center and one off of center, and analyzed using the procedures of Jensen et al. [10]. Both PDV traces were found to be identical on each of the three Ta spallation experiments.

The Ta specimens following loading were cross-sectioned and prepared for optical metallography and electron backscatter diffraction (EBSD) [12]. Automated EBSD scans were performed with a step size of 0.11 mm in a hexagonal grid at 20 kV in an FEI XL30 FEG-SEM equipped with TSL data acquisition hardware and software. Analysis of EBSD data provided crystal orientation information, as well as spatial misorientation distribution associated with the void damage field. X-ray microtomography measurements were carried out using an Xradia MicroXCT which was equipped with a 150 keV sealed tungsten high-energy microfocus X-ray source and a 2048 × 2048 pixel 16-bit high resolution cooled CCD detector. Owing to the high X-ray absorption of tantalum, small matchstick samples of cross-section 0.6 × 0.6 mm^2 were required to ensure adequate transmission of X-rays in the projections. These were cut from the 10.6 GPa shocked Ta sample such that the long axis represented the thickness of the impacted target. The tomography figures were calculated by segmenting the reconstructed X-ray tomography volumes based on grey level, therefore separating the

voids from the sample bulk. By selecting a single voxel within a void, all connected voxels to this, within a specified grey level range, are also automatically selected, ensuring the shape of the void to be defined by the boundary between the void and the metal phase. Applying this for each of the voids within the scanned region-of-interest (ROI), having a height of 1.1 mm, results in a segmented volume of voids, that can be displayed as a 3-D surface plot.

3. Results and Discussion

3.1. Free Surface Velocity Profiles

The free surface velocity (FSV) profiles for the experiments are shown in figure 1. These measurements were performed at the sample back free surface. All three loading profiles exhibit a pronounced Hugoniot Elastic Limit (HEL) at ~50 m/s. The three spallation experiments reach peak shock stresses in the Ta targets of 7.4, 10.6, and 21 GPa, respectively while displaying differing pulse durations of ~0.84, ~0.28 and ~0.25 μs, respectively as a consequence of the differing impactor designs utilized. The highest peak stress loaded spall sample (21 GPa) resulted in full spallation, i.e., a scab was ejected off the rear of the sample, while the 7.4 and 10.6 peak stress tests resulted in incipient spall damage in the recovered samples. The magnitude of the apparent "pull-back" signals, denoted by the red arrowed lines superimposed on the FSV profiles, are however seen to be essentially identical for each of the three experiments while the peak shock stresses and pulse durations at peak stress are substantially different. For this shot, utilizing the standard straight impedance spall drop relationship proposed by Novikov [13] where: $\sigma_{spall} = \frac{1}{2}\rho_0 c_B(\Delta FSV)$ yields spall strengths of 4.71, 4.7, and 5.2 GPa, respectively for the three Ta spall shots. For the highest peak stress test, 21 GPa, where a complete spall scab was formed, the dynamic impedance can be corrected using $\sigma_{spall} = \frac{1}{2}\rho_0 c_B(\Delta FSV + \delta)$ as proposed by Kanel [14] resulting in a corrected spall strength of 4.85.

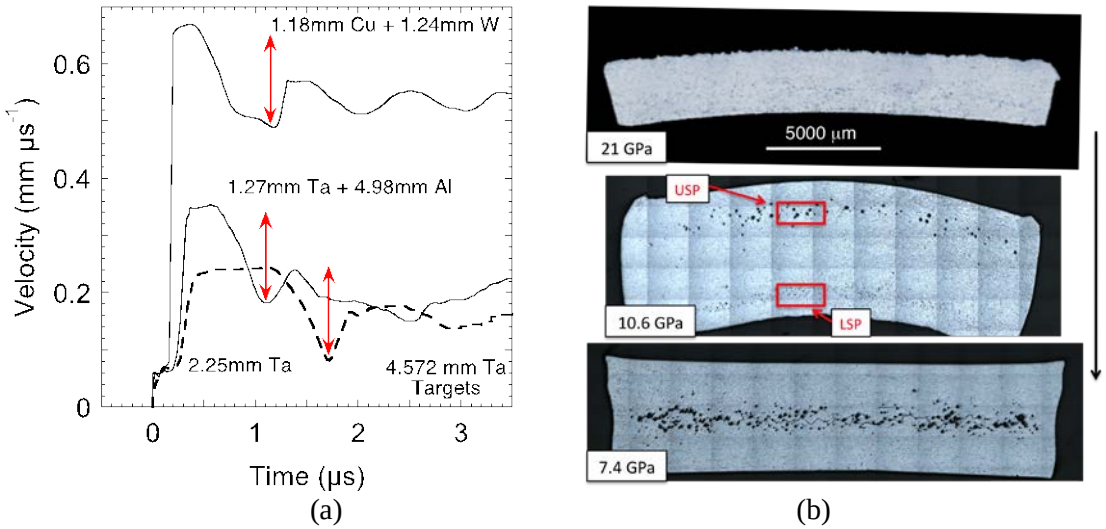

Figure 1. a) Traces of the free surface velocity for the three different peak stress / impactor configurations, and b) macroscopic thru-thickness cross-sectional views of the three Ta samples shocked to 7.4, 10.6, and 21 GPa. (Shock-loading direction as indicated by arrow in figure.)

3.2. Post-Mortem Metallurgical Analysis

The damage evolution in the three Ta samples was seen to vary as a function of the varying peak shock stresses and pulse durations while nominally exhibiting roughly similar "pull-back" signals. Figure 1b shows thru-thickness macroscopic optical micrographs of the three Ta spallation samples.

The sample loaded to a peak shock stress of 21 GPa is seen to have fully spalled into two pieces (only the lower half is shown in figure 1b), while the 10.6 and 7.4 GPa loaded samples exhibit macroscopic incipient spall damage. The Ta-Ta symmetrically impacted sample loaded to 7.4 GPa displays a well-developed field of voids located mid-plane in the sample. A representative area showing very intense and complex localization linkages connecting the voids is shown in figure 2a. Large lattice rotations of up to 45 degrees are evident in the grains adjacent to the linkages. Isolated fine twins are seen throughout the microstructure. The sample loaded with the composite impactor to 10.6 GPa peak stress displays two incipient damage fields, termed the upper and lower spall plane regions (figures 2b, 3a, and 3b). A field of isolated ~ 50- to 100-μm sized voids located roughly 1-mm from the upper sample surface is seen in the upper spall plane of the sample and an additional field of numerous small, <50 μm, void nucleation sites as seen in figure 3a is seen within 1-mm of the lower sample surface. The primary, USP, damage field displays very few localization linkages connecting the voids, isolated fine twins, and intragranular lattice rotations of up to 35 degrees in the grains adjacent to the voids. The lower damage field displays more extensive deformation throughout the region with most grains affected by deformation, no evidence of deformation twinning, extensive deformation near grain boundaries, and intragranular lattice rotations across the region of 35 degrees as seen in figures 3a and 3b. Figure 3a provides a unique view into the details of void nucleation in the lower spall plane. The anisotropic distribution of dislocation slip bands / localized shear features all located at or near grain boundaries identifies grain boundaries as the preferred nucleation damage sites for incipient spall in these nominally 1-D spall experiments on high-purity Ta. Tomography of the upper and lower spall plane regions was found to exhibit voids consistent with the optical metallography as seen in figures 4a and 4b. Within the regions of interest selected, the void volume fractions were measured to be 1.23% and 0.08% within the upper and lower spall planes, respectively.

Finally, the sample loaded to a peak shock stress of 21 GPa displayed full spall with ductile fracture separating the sample into two pieces with plasticity and intense damage directly adjacent to the fracture surface as seen in figure 4c. Some isolated small voids are seen at grain boundaries away from the fracture surface in addition to isolated deformation twins adjacent to the fracture surface. The zone of damage is concentrated within 500 microns of the fracture surface and many of the voids were seen at grain boundaries and coalescence of these is effectively “unzipping” the material along the boundaries.

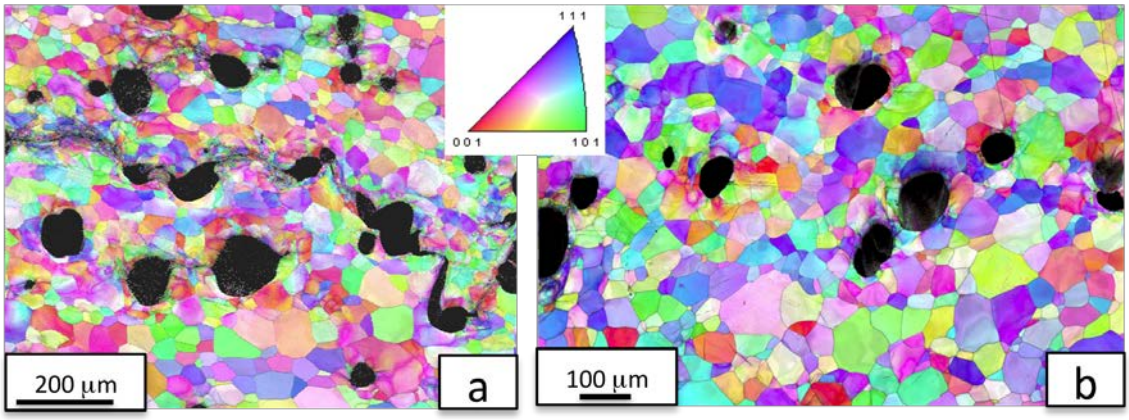

Figure 2. Crystal direction map of: a) the 7.4 GPa sample showing well-formed spherical voids with intense localization linkages between voids, and b) the 10.6 GPa sample at the upper spall plane USP (see figure 1b) showing voids with very few localization linkages from primary damage area.

Taken collectively, the velocimetry and post-mortem metallurgical analysis of the spallation samples provides some interesting insights into the damage evolution and spallation mechanisms operative in Ta for the shock drive imposed. To first order, the fact that the three different peak shock stresses when subjected to nearly identical tensile pulses resulted in essentially the same “pull-back”

signals supports minimal peak-stress or rate-dependent strain hardening or shock hardening on the damage evolution in Ta. This finding is consistent with the lack of rate dependent strain hardening as well as the lack of enhanced shock hardening previously linked to planar dislocation glide and the high Peierls-Nabarro stress in Ta [15]. Examination of the details of the damage evolution of the three spall samples illustrates that in Ta under the imposed nominally 1-D loading: 1) initial damage nucleation occurs via anisotropic slip / shear at selected grain boundaries in a heterogeneous manner (figures 3a and 3b), 2) initial void growth leads to ~spherical voids reflecting the local hydrostatic loading, and 3) void coalescence in adjacent voids occurs via pronounced shear localization.

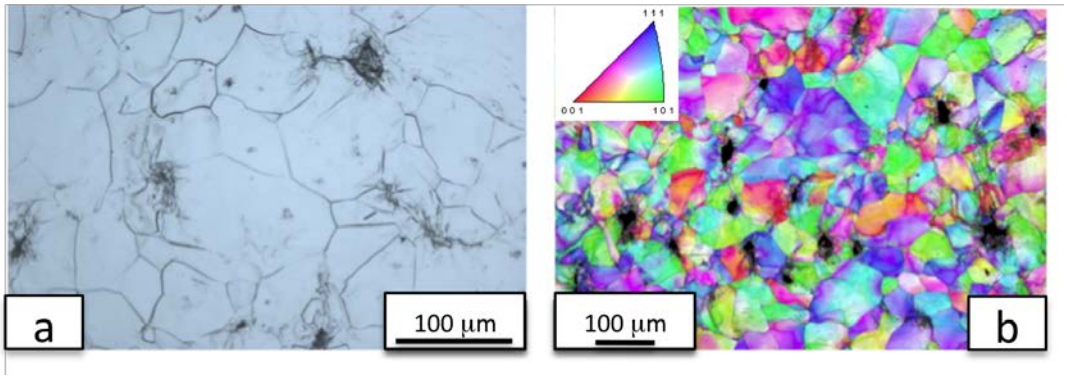

Figure 3. Lower spall plane (LSP) 10.6 GPa sample showing localized plasticity vortices within extensive deformation-affected grains serving as nucleation sites for small incipient voids as viewed using a) optical metallography – etched sample, and b) EBSD imaging.

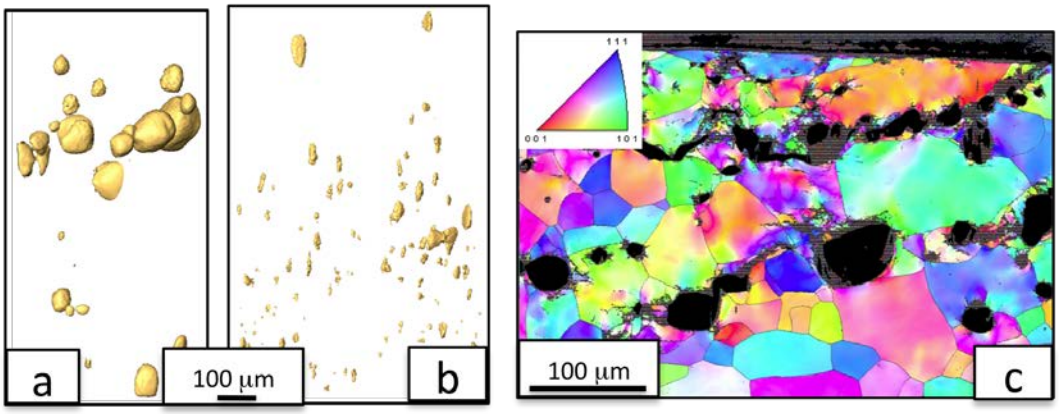

Figure 4. a) tomography of voids in 10.6 GPa sample upper spall plane, and b) tomography of lower spall plane in 10.6 GPa sample, c) crystal direction map for the 21 GPa sample exhibiting voids and extensive deformation-affected grains just below the complete fracture surface.

The observation of damage nucleation leading to voids located at grain boundaries in the current study is radically different than the observation of void formation occurring preferentially at deformation twin-twin intersections or at twin-grain boundary intersections [8] in Ta shocked via a sweeping detonation wave. The increased propensity for twin formation during sweeping-detonation-wave loading, at a peak shock stress nominally similar to the 10.6 GPa current nominally 1-D Ta sample loading, reinforces the importance of shock obliquity, and its commensurate higher shear stresses, with increased shock obliquity increasing deformation twin formation propensity and thereafter damage nucleation mechanisms during spallation. Finally, the essentially identical “pull-back” signals, resulting from the three different shock-loading histories which display different evolved damage fields, illustrates the lack of uniqueness of a given “pull-back” spall signal magnitude

obtained from rear-surface velocimetry to quantifying shock-induced spall- and shock-induced damage evolution in materials.

4. Summary

Tantalum samples shock loaded to three different peak shock stresses and shock pulse durations were subjected to nearly identical tensile pulses using both symmetric impact, and two different composite flyer plate configurations. The three different loading paths were seen to display: 1) nearly identical "pull-back" signals as measured via rear-surface velocimetry and 2) different evolved damage fields. These two observations illustrate the lack of uniqueness of a fixed "pull-back" spall signal magnitude obtained from rear-surface velocimetry to the quantification of spall strength and shock-induced damage evolution for a given material as uniquely linked to a fixed spall strength value.

Acknowledgements

Los Alamos National Laboratory is operated by LANS, LLC, for the NNSA of the US Department of Energy under Contract No. DE-AC52-06NA25396. This research was supported under the auspices of the US Department of Energy and the Joint DoD/DOE Munitions Program.

References

[1] Rinehart J S and Pearson J 1954 Behavior of Metals under Impulsive Loads (Cleveland, Ohio:American Society for Metals)
[2] Johnson J N 1981 *J. Appl. Phys.* **52** 2812
[3] Meyers M A and Aimone, C T 1983 *Prog. Mater. Sci.* **28** 1
[4] Gray III G T, Bourne N K and Henrie B L 2007 *J. Appl. Phys.* **101** 093507
[5] Rinehart J S 1952 *J. Appl. Phys.* **23** 1229
[6] Butcher B M, Barker L M, Munson D E, and Lundergan C D 1964 *AIAA Journal* **2** 977
[7] Escobedo J P, Brown E N, Trujillo C P, Cerreta E K and Gray III G T 2013 *J. Appl. Phys.* **113** 103506
[8] Gray III G T, Hull L M, Livescu V, Faulkner J R, Briggs M E and Cerreta E K 2012 *DYMAT 2012 - 10th International Conference on the Mechanical and Physical Behaviour of Materials Under Dynamic Loading* edited by (EDP Sciences, Freiburg, Germany) pp 02004
[9] Gray III G T, Livescu V, Cerreta E K, Mason T A, Maudlin P J and Bingert J A 2009 *DYMAT 2009: 9th International Conference on the Mechanical and Physical Behaviour of Materials Under Dynamic Loading* edited by (EDP Sciences, Brussels, BELGIUM) pp 963
[10] Jensen B J, Holtkamp D B, Rigg P A and Dolan D H 2007 *J. Appl. Phys.* **101** 013523
[11] Gray III, G T 2000 Shock wave testing of ductile materials (Materials Park, Ohio:ASM International)
[12] Adams B L, Wright S I and Kunze K 1993 *Metallurgical Transactions* A **24A** 819
[13] Novikov S A, Divnov I I and Ivanov A G 1966 *Phys. Metals Metallog.* **21(4)** 122
[14] Kanel G I 2001 *J. Appl. Mech. Tech. Phys.* **42** 358
[15] Gray III G T and Vecchio K S 1995 *Metall. Mater. Trans.* A **26** 2555